

COORDINATE SYSTEMS FOR ANALYSIS OF ON-ORBIT CHANDRA DATA PAPER I: IMAGING

JONATHAN MCDOWELL
Harvard-Smithsonian Center for Astrophysics

2001 May 13

1 Introduction

The Chandra X-ray Observatory, launched in July 1999, provides X-ray imaging and spectral data of unprecedented, subarcsecond, resolution. The geometry of Chandra's detectors is more complicated than those of previous missions; this, coupled with the higher accuracy requirements, means that more care must be taken to derive accurate coordinates and to distinguish clearly between different coordinate systems.

This revision includes the values current in the processing system as of that date. Revised values are currently being evaluated by the CXC calibration group.

There are important operational differences between imaging performed by X-ray telescopes and those performed by optical telescopes, even spaceborne ones such as the Hubble Space Telescope. An optical telescope will typically track its target, and accumulate counts in an image. Any variation in the telescope's pointing direction will degrade the final image quality. In contrast, an X-ray telescope's pointing direction varies slightly with time, deliberately smearing the target source's image over different parts of the detector. The image is then reconstructed by adjusting the positions of each photon by taking into account the exact pointing direction of the spacecraft at the photon's arrival time ("aspect correction"). This image reconstruction is possible because the fundamental X-ray data product is not an image but an 'event list' in which the positions and arrival times of individual photons are recorded.

In the first part of this paper I discuss the general problem of obtaining celestial coordinates from the telemetered data. In the second section, I define the coordinate systems precisely, presenting the transformation equations used to convert between them. The final part of the paper gives specific values for in-flight data from the Chandra Observatory.

1.1 Fundamentals

The Chandra X-ray Observatory has a single Wolter I imaging telescope, the HRMA (High Resolution Mirror Array) with four nested mirror pairs. The HRMA focusses X-rays onto a detector in the ISIM (Integrated Science Instrument Module); one of two transmission grating assemblies may be placed in the beam to disperse the image for spectroscopic studies. In this paper I consider only non-dispersed images. There are two focal plane instruments in the ISIM, the ACIS (Advanced CCD Imaging Spectrometer) and the HRC (High Resolution Camera). The HRC is made up of

two microchannel plane detectors, the imaging HRC-I and the long HRC-S array used mostly as a spectroscopy detector. ACIS also has imaging and spectroscopic arrays, but for the purposes of data analysis we consider ACIS to be a single detector, since unlike HRC its chips may be read out in any combination. The detectors are mounted on a movable optical bench, the SIM (Science Instrument Module). The SIM can move in both the focus (X) direction and along the axis (Z) separating the detectors; this axis is perpendicular to the dispersion axis (Y). In initial operations there are four standard Z positions for the SIM, but non-standard positions may also be commanded.

In the idealization adopted in this paper, each of the three detectors HRC-S, HRC-I and ACIS consists of a number of finite rectangular detector planes or ‘logical chips’ (the correct term for HRC is ‘segment’ but we will use the term chip generically to refer to a semiconductor chip, a microchannel plate segment, a proportional counter, a photographic plate or any other finite rectangular plane). In Chandra, these chips are oriented approximately along the best focal surface, in contrast to previous X-ray telescopes in which the chips were normal to the optical axis. The chips are considered to consist of a rectangular array of identical rectangular (in practice square) chip pixels. For ACIS, these chip pixels are the physical pixels of the CCD, while for HRC they represent a conventional, artificial pixelization employed by the instrument’s position calculation algorithm. In this paper we take the chip coordinates as given and assume all nonlinearities and detector effects have already been removed. Typically the chip coordinates are integers, but this is not required (grade-based event finding algorithms could give fractional chip positions even for the physically real pixels of ACIS). The logical chip plane may be larger than the active area of the detector (for the ROSAT PSPC, the logical plane is a rectangle containing the actual detector, which is circular).

1.2 The chip, detector and sky coordinate systems

There are then three fundamental coordinate systems which must be considered in analysing such an event list. In the ‘chip’ coordinate system, we consider the position of the photon in the chip plane, corrected for all detector effects. In the ‘focal plane’ or ‘detector’ space, the position of the photon in the tangent plane to the optical axis is considered; and in the ‘sky’ coordinate system, we record the position of the photon in the fictitious tangent plane to a nominal fixed celestial pointing direction. These three systems are useful for considering different effects: in the chip system, stars will be smeared out but bad pixels and chip boundaries will be well defined, while in the sky system stars will be pointlike and bad pixels will be smeared out. The position of the photons in the detector system tells you the off-axis angle, allowing you to calculate mirror-based effects such as point spread function and vignetting. The name ‘detector’ for this coordinate system is a misnomer, but is retained for compatibility with earlier instruments such as ROSAT in which chip and detector coordinates were identical.

In principle we can distinguish between the focal plane system (tangent plane to the optical axis at the detector end of the telescope) and an incoming tangent plane system (tangent plane at the sky end of the mirrors); these differ because the mirror is not a perfect point lens. We choose instead to identify the incoming tangent plane and focal plane systems, and handle mirror effects by using the point spread function formalism. In particular, any variations in angular deflection across the field are assumed to be absorbed in an offset of the point spread function’s origin relative to its centroid. In practice for Chandra ray trace simulations demonstrate that this effect can be neglected. For the calculation of coordinates, the fact that the telescope consists of multiple optical assemblies with different optical axes and focal lengths is entirely ignored; we adopt a single nominal optical axis and plate scale, and absorb the complexities of the actual optical system into the point spread function.

To convert from chip to detector coordinates, we must correct for the position of the chips in three-dimensional space on the SIM (optical bench), for the translation position of the SIM in X

and Z, and for any misalignment of the SIM Z axis with the aspect camera axis. We also allow six degrees of freedom for time-dependent warping of the telescope structure due to thermal effects, moving the SIM frame relative to the mirror axes. In practice, only three of these degrees of freedom are measured (and contribute motions of the order of 1 arcsecond during an observation) and the remaining three are assumed to have a negligible effect. We must also know the origins of the instrument coordinate systems accurately with respect to the telescope optical axis; there are still significant uncertainties in these values, which will be improved with continuing analysis of on-orbit data.

To convert from detector to sky coordinates, we simply apply the time dependent ‘aspect solution’, that is, the RA and Dec of the optical axis and the roll angle of the spacecraft axes with respect to the celestial meridian versus time. Applying the aspect solution involves reprojecting the photons from the tangent plane of the instantaneous pointing direction to the tangent plane of the nominal pointing direction. In previous missions the calculation has been simplified by using fixed translational offsets for the whole field, and this approximation is also used in early Chandra data processing. However it is not quite good enough for full accuracy, and will in future be replaced by the full calculation.

The Chandra observatory is ‘dithered’ with a deliberate periodic Lissajous oscillation tracing out an approximately square region on the sky with an amplitude of 15 arcseconds. A single star tracker camera is used to determine the pointing direction as a function of time. The offset between the star tracker and the telescope optical axis must be calibrated with on-orbit observations. This procedure is discussed in Paper 2.

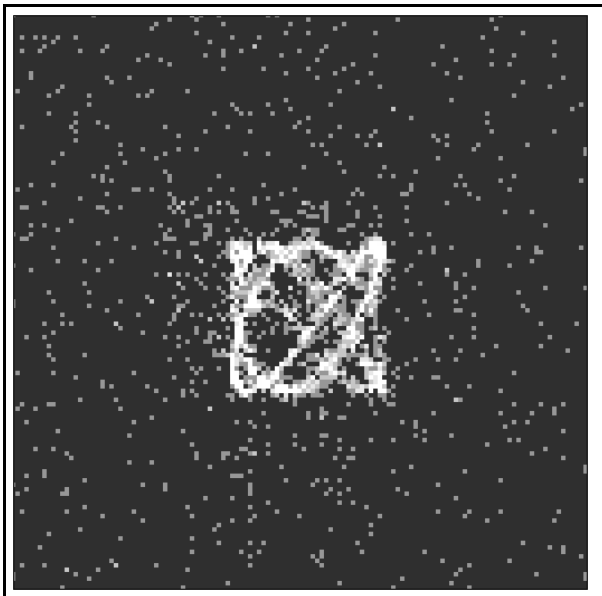


Figure 1: An image in detector coordinates, showing a dithered source.

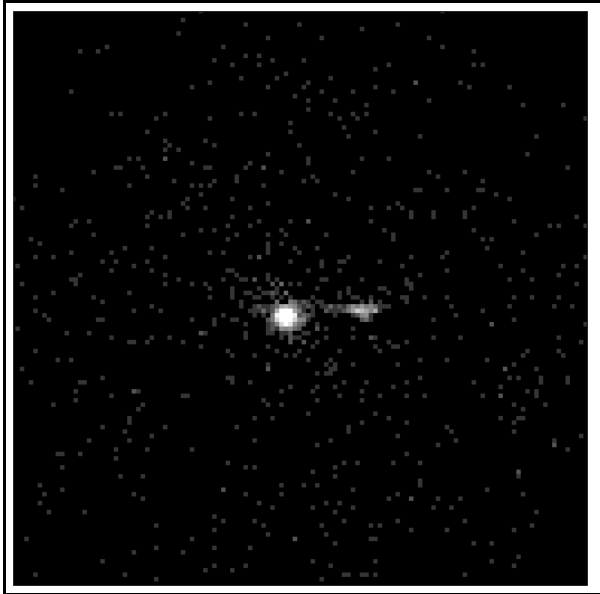


Figure 2: The same image in sky coordinates, with aspect applied. The source is PKS 0637-752, a quasar with a newly discovered X-ray jet.

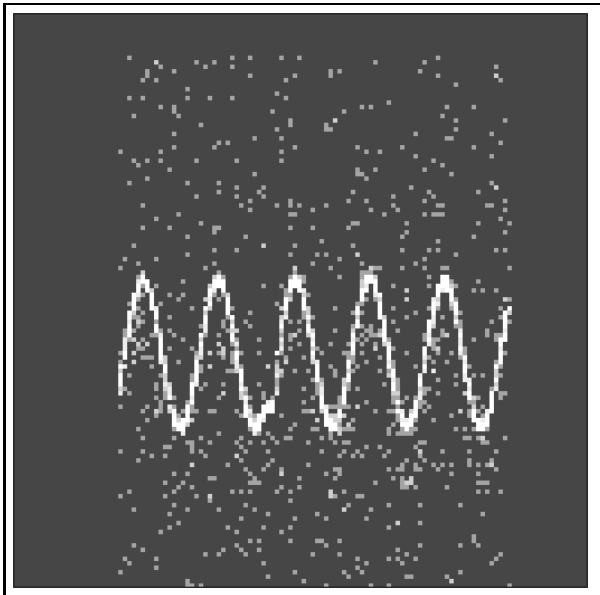


Figure 3: The same image showing DETX versus time along the x axis

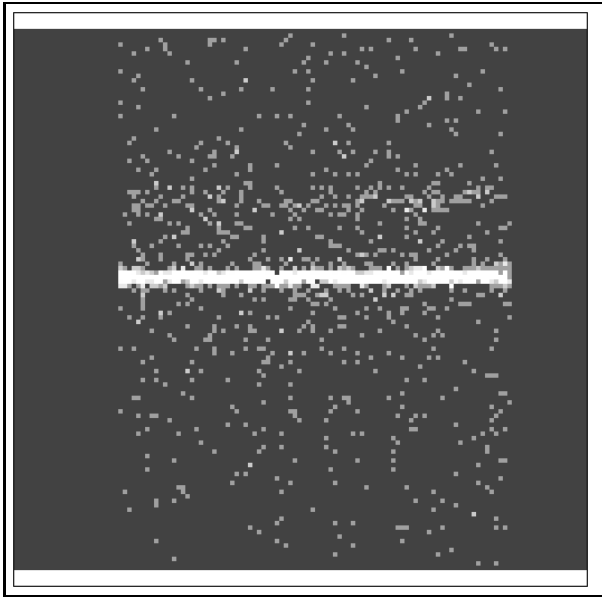


Figure 4: The same image showing the X coordinate on the y axis versus time along the x axis. The jet is visible at larger X values.

Because of the tilting of the individual chips and the dithering of the optical axis, and the possibility of changing focal length, individual physical pixels in chip space do not correspond directly to pixels in detector and sky space, and we are free to choose entirely different units for these coordinate frames. We retain the concept of ‘pixels’ since it is convenient and conventional to have a standard pixelization for image analysis. However, while the sizes of chip pixels are defined in millimeters, the sizes of detector and sky pixels are defined to be a fixed number of arcseconds. In practice we adopt conventional pixel sizes for the detector and sky coordinate systems which have the same size as chip pixels when the detector is at the nominal focus. In the event lists, the detector and sky coordinate values are retained as floating point values in pixel units. To avoid aliasing effects when making images, the calculation of detector coordinates in standard processing introduces a uniform randomization of ± 0.5 pixel in the integral chip coordinate value, representing the fact that uniformity is a reasonable prior for the probability distribution of the exact location the photon fell within the chip pixel.

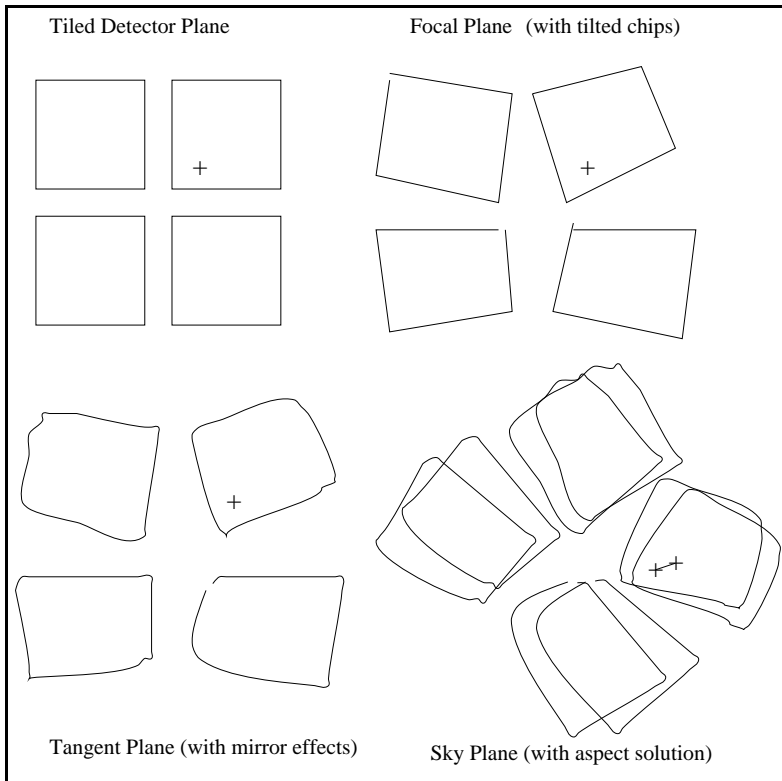


Figure 5: The different pixel plane coordinate systems. Distorting effects are highly exaggerated.

In Chandra FITS files, the chip, detector and sky pixel systems are stored in the (CHIPX,CHIPY), (DETX,DETY) and (X,Y) columns respectively. For a given detector, there may be more than one chip, each with its own chip coordinate system. We therefore also define a ‘tiled detector coordinate system’, (TDETX,TDETY) which combines chip coordinate and chip number to provide a single system covering all the chips. Unlike DET, the TDET system does not retain the true 3D spatial relationship between the chips, but does retain the identity of individual chip pixels. It may therefore be an appropriate system to use when filtering out bad pixels.

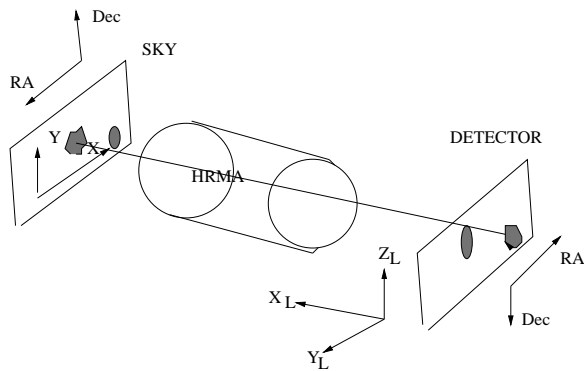


Figure 6: Imaging the sky in LSI coordinates

1.3 Pixel convention

In all cases where we use discrete **pixel numbers**, the corresponding real-valued, continuous **pixel coordinates** are defined to be equal to the pixel number at the center of the pixel. We further recommend that for finite detector planes, one corner be designated as the lower left corner, LL. Then the pixel which has LL as one of its corners (i.e. the lower left pixel) shall be numbered (1,1) so that its center has coordinates (1.0, 1.0). The coordinates of the LL point itself are (0.5, 0.5). If the detector is rectangular with sides of length XMAX, YMAX the pixel coordinates then run from (0.5, 0.5) in the lower left corner (LL) to (XMAX+0.5, YMAX+0.5) in the upper right corner (UR) while the pixel numbers in each axis run from 1 to XMAX, 1 to YMAX. These conventions are consistent with established practice in archival X-ray FITS event lists.

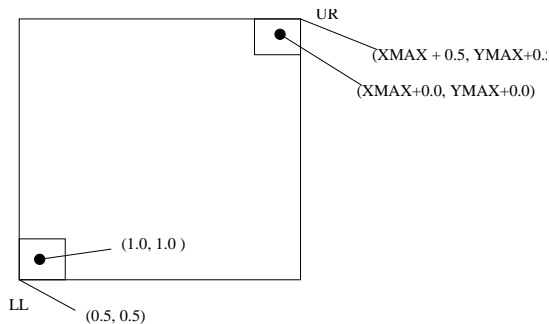


Figure 7: Pixel convention.

2 Transformation equations and intermediate coordinate systems

2.1 Sky coordinates to celestial coordinates

The sky coordinate system X,Y is defined by a reference pixel X₀,Y₀, the world coordinates at that reference point α_0, δ_0 and their first derivatives at that point Δ_X, Δ_Y . We choose square pixels so

that

$$-\Delta_X = +\Delta_Y = \Delta$$

The minus sign on the X derivative arises because we are on the inside of the celestial sphere looking out, so that right ascension increases to the left, which is -X on the image.

To convert from tangent plane pixels X,Y to actual celestial coordinates α, δ , first calculate scaled coordinates (note that Δ must be expressed in radians per pixel here)

$$\begin{pmatrix} x \\ y \end{pmatrix} = \begin{pmatrix} -\Delta(X - X0) \\ \Delta(Y - Y0) \end{pmatrix}$$

and then the local angular coordinates.

$$\phi = \arg(x, -y)$$

and

$$\theta = \arg(1.0, \sqrt{x^2 + y^2})$$

Finally convert local angular coordinates to world coordinates by rotating through Euler angles $(\alpha_0, \pi/2 - \delta_0, \pi)$ as follows:

$$\alpha = \alpha_0 + \arg(-\cos \theta \sin \phi, \sin \theta \cos \delta_0 - \cos \theta \sin \delta_0 \cos \phi)$$

and

$$\sin \delta = \sin \theta * \sin \delta_0 + \cos \theta \cos \delta_0 \cos \phi$$

The inverse calculation: Rotate the world coordinates forward through the same Euler angles:

$$\phi = \pi + \arg(-\cos \delta \sin(\alpha - \alpha_0), \sin \delta \cos \delta_0 - \cos \delta \sin \delta_0 \cos(\alpha - \alpha_0))$$

and

$$\sin \theta = \sin \delta \cos \delta_0 + \cos \delta \sin \delta_0 \cos(\alpha - \alpha_0)$$

Then let

$$\begin{pmatrix} x \\ y \end{pmatrix} = \cot \theta \begin{pmatrix} \sin \phi \\ -\cos \phi \end{pmatrix}$$

and

$$\begin{pmatrix} X \\ Y \end{pmatrix} = \begin{pmatrix} X0 - x/\Delta \\ Y0 + y/\Delta \end{pmatrix}$$

2.2 Detector coordinates to celestial coordinates

The procedure for mapping detector to celestial coordinates is the same with the addition of a rotation through the spacecraft roll angle γ . In this case α_0, δ_0 are the coordinates of the instantaneous pointing direction.

To convert from tangent plane pixels DETX,DETY to actual celestial coordinates α, δ , first calculate scaled coordinates (note that Δ must be expressed in radians per pixel here)

$$\begin{pmatrix} x \\ y \end{pmatrix} = \Delta \begin{pmatrix} -(X - X0) \cos \gamma - (Y - Y0) \sin \gamma \\ -(X - X0) \sin \gamma + (Y - Y0) \cos \gamma \end{pmatrix}$$

and then the local angular coordinates.

$$\phi = \arg(x, -y)$$

and

$$\theta = \arg(1.0, \sqrt{x^2 + y^2})$$

Finally convert local angular coordinates to world coordinates by rotating through Euler angles $(\alpha_0, \pi/2 - \delta_0, \pi)$ as follows:

$$\alpha = \alpha_0 + \arg(-\cos \theta \sin \phi, \sin \theta \cos \delta_0 - \cos \theta \sin \delta_0 \cos \phi)$$

and

$$\sin \delta = \sin \theta * \sin \delta_0 + \cos \theta \cos \delta_0 \cos \phi$$

2.3 Chip coordinates to detector coordinates

Recall that chip pixel coordinates run from (0.5,0.5) to (XMAX+0.5,YMAX+0.5) on the chip. We introduce several intermediate coordinate systems in three dimensions (and specified to be evaluated in millimeters)

1. the Chip Physical Coordinate (CPC) system, whose Z axis is normal to the chip, and whose origin coincides with chip coordinates (0.5,0.5).
2. the Local Science Instrument (LSI) system whose origin is at a conventional point on the detector and whose axes are approximately aligned with the spacecraft axes.

The four corners of each chip are specified in three dimensions in the LSI frame. The CPC to LSI rotation matrix is made up from the unit vectors in LSI coordinates of the CPC axes.

Let us denote the position vectors of the four chip corners as $\mathbf{LL}, \mathbf{UL}, \mathbf{UR}, \mathbf{LR}$. Then the unit vectors of the CPC origin and axes in LSI coordinates are

$$\mathbf{p}_0 = \mathbf{LL}, \mathbf{e}_X = \mathbf{LR} - \mathbf{LL}, \mathbf{e}_Y = \mathbf{UL} - \mathbf{LL} \quad (1)$$

and

$$\mathbf{e}_Z = \mathbf{e}_X \wedge \mathbf{e}_Y. \quad (2)$$

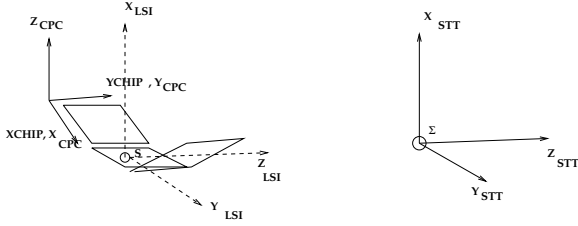


Figure 8: The relationship between CHIP, LSI and STT coordinates.

$$\begin{pmatrix} X_{LSI} \\ Y_{LSI} \\ Z_{LSI} \end{pmatrix} = \begin{pmatrix} X_{LL} \\ Y_{LL} \\ Z_{LL} \end{pmatrix} \begin{pmatrix} (\mathbf{e}_X)_X & (\mathbf{e}_Y)_X & (\mathbf{e}_Z)_X \\ (\mathbf{e}_X)_Y & (\mathbf{e}_Y)_Y & (\mathbf{e}_Z)_Y \\ (\mathbf{e}_X)_Z & (\mathbf{e}_Y)_Z & (\mathbf{e}_Z)_Z \end{pmatrix} \begin{pmatrix} X_{CPC} \\ Y_{CPC} \\ Z_{CPC} \end{pmatrix}$$

3. The LSI coordinate system must now be related to the SIM Translation Table (STT) and SIM Translation Frame (STF) coordinate system, which respectively take into account the position of the instrument on the optical bench and the current position to which the bench has been

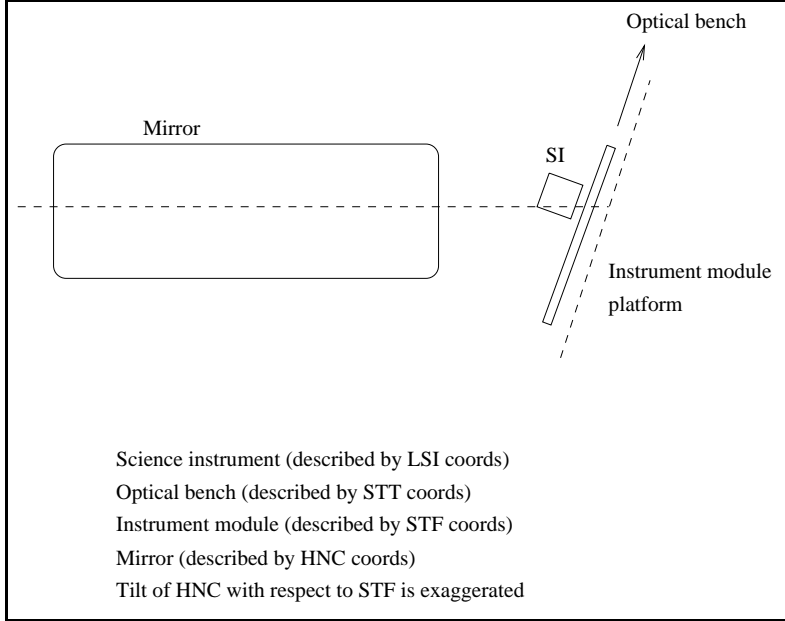


Figure 9: The instrument compartment (dashed line) may be misaligned with the telescope mirrors. At calibration, this misalignment (highly exaggerated here) may be significant and variable as the mirror is tilted with respect to the instruments. The instrument bench moves with respect to the instrument compartment, as indicated by the arrow.

moved. The STT coordinate system is fixed in the optical bench, while the STF coordinate system is fixed in the ISIM module. We record the position of each instrument's LSI origin OLSI on the optical bench by giving the position of OLSI in STT coordinates. We also allow for a possible angular misalignment of the LSI system through a small angle λ_i by defining 'corrected LSI coordinates'

$$\begin{pmatrix} X'_{LSI} \\ Y'_{LSI} \\ Z'_{LSI} \end{pmatrix} = \begin{pmatrix} 1 & 0 & 0 \\ 0 & \cos \lambda_i & -\sin \lambda_i \\ 0 & \sin \lambda_i & \cos \lambda_i \end{pmatrix} \begin{pmatrix} X_{LSI} \\ Y_{LSI} \\ Z_{LSI} \end{pmatrix}$$

chosen so that the corrected LSI axes of all the detectors line up. In practice we plan to recalculate the chip corners in this corrected LSI space once the alignment angles are known, and omit use of the 'raw' LSI values.

The coordinates of a pixel in STF coordinates are obtained by adding the instrument origin coordinates OLSI and the current SIM translation position to the LSI coordinates. OLSI also gives the STF coordinates of the instrument's LSI origin when the SIM(X,Y,Z) value is zero; in other words, the origins of STT and STF are defined to coincide when the SIM is at its zero position.

$$\begin{pmatrix} X_{STF} \\ Y_{STF} \\ Z_{STF} \end{pmatrix} = \begin{pmatrix} X'_{LSI} \\ Y'_{LSI} \\ Z'_{LSI} \end{pmatrix} + \begin{pmatrix} SIM_X \\ SIM_Y \\ SIM_Z \end{pmatrix} + \begin{pmatrix} OLSI_X \\ OLSI_Y \\ OLSI_Z \end{pmatrix}$$

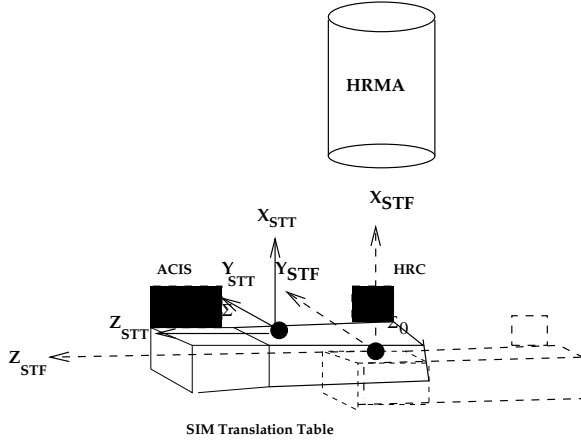


Figure 10: The relationship between STT and STF coordinates, AXAF example. The instrument (SIM) table has moved so that HRC is at the focus.

4. The focal coordinate (FC) system is fixed in the HRMA and centered on the telescope's nominal focus. The origin of FC and STF coordinates is nominally the same, but time-dependent shifts in the spacecraft structure require corrections:

$$\begin{pmatrix} FCX \\ FCY \\ FCZ \end{pmatrix} = \begin{pmatrix} dX_{STF} \\ dY_{STF} \\ dZ_{STF} \end{pmatrix} R_E(\psi_X, \psi_Y, \psi_Z) \begin{pmatrix} X_{STF} \\ Y_{STF} \\ Z_{STF} \end{pmatrix}$$

where R_E is a rotation matrix. The angles ψ_Y and ψ_Z and the focal shift dX have only a tiny effect on the celestial coordinates, and in the case of Chandra they are both not measured and neglected. The angle ψ_X (an additional roll of the detector module relative to the mirrors) and the translational shifts dY , dZ are measured by observations of the fiducial lights mounted on the instruments. In the case of Chandra, they are reported on a time resolution of about one second and have a typical magnitude of a few tenths of an arcsecond.

5. We now correct to the nominal mirror node, adopting Mirror Nodal Coordinates (MNC)

$$\begin{pmatrix} MNX \\ MNY \\ MNZ \end{pmatrix} = \begin{pmatrix} FCX - f \\ FCY \\ FCZ \end{pmatrix}$$

where f is the nominal focal length. Chandra has four mirror shells, each of which has a different optical node and focal length; we adopt a nominal mean node and focal length and absorb deviations from this into the energy and position dependent mirror point spread function. Note that MNX is large and negative for a position near the focus.

6. finally, the detector (focal plane pixel) coordinates are calculated from the focal coordinates by

$$\begin{pmatrix} DETX \\ DETY \end{pmatrix} = \begin{pmatrix} X0 - \Delta MNY/MNX \\ Y0 + \Delta MNZ/MNX \end{pmatrix}$$

2.4 Detector coordinates and off-axis angles

The optical axis of the telescope is defined to lie at the reference pixel X0, Y0 in detector coordinates, chosen to be the center of the image. (However, users are warned that in early data processing the position of the optical axis is not known, and so coordinates in this system will be revised).

We define Mirror Spherical Coordinates (r, θ_H, ϕ_H) in terms of mirror nodal Cartesian coordinates as follows:

$$\begin{pmatrix} X_N \\ Y_N \\ Z_N \end{pmatrix} = \begin{pmatrix} r \cos \theta_H \\ r \sin \theta_H \cos \phi_H \\ r \sin \theta_H \sin \phi_H \end{pmatrix} \quad (3)$$

The angle θ_H is the **MSC off-axis angle** and ϕ_H is the **MSC Azimuth**. The inverse is

$$\begin{aligned} r &= \sqrt{X_N^2 + Y_N^2 + Z_N^2} \\ \theta_H &= \cos^{-1}(X_N/r) \\ \phi_H &= \arg(Y_N, Z_N) \end{aligned} \quad (4)$$

2.5 Dithered-corrected chip (DC) and chip-aligned source-centered sky (CSC) coordinates

The systems described in this subsection have not yet been implemented in the CXC data processing system.

In ACIS ‘continuous clocking’ mode, only the CHIPX coordinate is available; CHIPY is unknown. In fact, if t_r is the time tag at readout and t is the actual event time,

$$t_r = t + \text{CHIPY} * dt$$

where dt is the time to clock out one row. To get accurate times and positions we must know the actual sky position of the source. The best we can do is to obtain a 1-dimensional profile of the source perpendicular to the readout direction. Because the ACIS-I and ACIS-S chips are at a variety of orientations, we can’t define a single 1-D coordinate in the sky frame which is well defined over multiple chips. Instead, we define new coordinates, the dither corrected chip system and the 1-D sky system. It is not possible to obtain corrected times and positions for photons not associated with a known source.

Let $A(t)$ be the aspect solution at time t (more precisely, the operator mapping chip to sky coordinates, which also includes the time dependent boresight and the SIM information). Define the reference aspect solution A_0 to be the nominal aspect solution (actually, you can use the time averaged aspect solution the aspect solution at some specific time instead; the time average would make the result more stable and would center the resulting image, but is more work to calculate).

Let (x_s, y_s) be the sky coordinates of a source. Then the chip coordinates of the source as a function of time are

$$(cx_{ref}(t), cy_{ref}(t)) = A^{-1}(t)(x_s, y_s, E(cx))$$

where $E(cx)$ reflects the dependence on predicted chip position of the photon energy for grating data. The reference chip coordinates are

$$(cx_s, cy_s) = A_0^{-1}(x_s, y_s)$$

We define the dither corrected chip coordinates for an event detected at cx, cy to be

$$(dcx, dcy) = (cx, cy) + (cx_s, cy_s) - (cx_{ref}(t), cy_{ref}(t))$$

This definition is meaningful for both TE and CC mode data for chips with the same orientation as the chip on which the source lies. It may be evaluated for other chips but the result will not be useful. In CC mode data, only the dcx coordinate can be evaluated, and we assume cy is at the expected position for the source $cy = cy_{ref}(t)$ so that $dcy = cy_s$.

The disadvantage of the dither corrected chip coordinates is that the sky angular positions are not preserved accurately. We define a source-centered, readout oriented, coordinate system, chip-aligned source sky coordinates (CSCX,CSCY) as follows. The positive CSCX axis lies in the direction from (x_s, y_s) to the point $(x_s + dx_s, x_s + dy_s)$ obtained by calculating the sky coordinates

$$(x, y) = A0(cx_s + \Delta, cy_s)$$

where Δ is an arbitrary positive increment of CHIPX. In words, we take the reference aspect and use it to project a line from the source parallel to CHIPX onto the sky plane. The source position is (CSCX0,CSCY0), chosen to have the same values as the reference position of the sky coordinate system (e.g. (4096.5,4096.5) for ACIS).

Then for each event, we apply the aspect solution to obtain sky coordinates

$$(x, y) = A(t)(cx, cy)$$

and calculate (CSCX,CSCY) with the appropriate rotation matrix. For CC mode and events on the target chip, CSCY is zero and

$$CSCX = CSCX0 + \sqrt{(x - x_s)^2 + (y - y_s)^2}$$

The (CSCX,CSCY) system is useful for a single chip (or for a set of chips which have exactly aligned readout directions, such as the ACIS-S array) and for a constant roll angle.

So in processing CC mode data, we:

- Calculate the reference aspect
- Calculate the sky position of the target
- Calculate the predicted chip position of the target at the reference aspect, (cx_s, cy_s)
- For each event at observed raw time t_r , chip id c and chip position (cx, cy) , calculate the predicted source chip position

$$(cx_{ref}(t), cy_{ref}(t)) = A^{-1}(t)(x_s, y_s)$$

and the dither correction $(\Delta cx, \Delta cy) = (cx_{ref}(t), cy_{ref}(t)) - (cx_s, cy_s)$ for the chip c , and calculate (dcx,dcy) if required.

- Calculate the corrected time assuming the photon is from the source

$$DCTIME = TIME - dt * cy_{ref}(t)$$

Recall there's no way of knowing the correct time for non-source photons.

- Optionally, recalculate $cy_{ref}(t), \Delta cx, \Delta cy$ and then (dcx,dcy), DCTIME using the aspect for DCTIME instead of TIME (necessary if the aspect solution changes measurably on a timescale DCTIME-TIME; one iteration should be sufficient).
- Calculate the predicted sky coordinates (x,y) from the observed cx and the calculated $cy_{ref}(t)$
- Calculate the final (CSCX,CSCY).

For grating data in CC mode, a more careful calculation should be done of the predicted dispersed photon chip Y coordinate as a function of chip X. We replace the equation

2.6 Source-centered coordinates

Another useful coordinate system is source-centered coordinates (SCX,SCY). Similar to CSCX,CSCY, the source-centered coordinates share the pixel size and reference position of the sky coordinate system, but are centered on a particular source and aligned with a specified source axis direction. The celestial coordinates of the source and direction of its axis may be specified as a function of time; the system is particularly intended for use with solar system targets. A world coordinate system giving position angle and angular distance from source center should be applied to the source-centered coordinates.

This system has not yet been implemented in the CXC data processing system.

3 In-flight numerical values for Chandra

3.1 ACIS and HRC chip locations

The ACIS instrument has 10 CCD chips. In the event list data, each is identified by an integer from 0 to 9. Four of the chips, the imaging set, are arranged in a rough square (but individually tilted). Six are the spectroscopic array, arranged in a line.

| Chip Name | CHIP ID |
|-----------|---------|
| ACIS-I0 | 0 |
| ACIS-I1 | 1 |
| ACIS-I2 | 2 |
| ACIS-I3 | 3 |
| ACIS-S0 | 4 |
| ACIS-S1 | 5 |
| ACIS-S2 | 6 |
| ACIS-S3 | 7 |
| ACIS-S4 | 8 |
| ACIS-S5 | 9 |

The CHIP ID is also called CCD ID for consistency with ASCA.

Table 2: ACIS Chip corner locations in ACIS-I LSI coordinates

| Chip | Corner | CPC coords | ACIS-I LSI coords |
|------|--------|---------------------|---------------------------|
| I0 | LL | (0.0, 0.0, 0.0) | (2.361, -26.484, 23.088) |
| | LR | (24.58, 0.0, 0.0) | (1.130, -26.546, -1.458) |
| | UR | (24.58, 24.58, 0.0) | (-0.100, -2.001, -1.458) |
| | UL | (0.0, 24.58, 0.0) | (1.130, -1.939, 23.088) |
| I1 | LL | (0.0, 0.0, 0.0) | (1.130, 23.086, -1.458) |
| | LR | (24.58, 0.0, 0.0) | (2.360, 23.024, 23.088) |
| | UR | (24.58, 24.58, 0.0) | (1.130, -1.521, 23.088) |
| | UL | (0.0, 24.58, 0.0) | (-0.100, -1.459, -1.458) |
| I2 | LL | (0.0, 0.0, 0.0) | (1.130, -26.546, -1.997) |
| | LR | (24.58, 0.0, 0.0) | (2.361, -26.484, -26.543) |
| | UR | (24.58, 24.58, 0.0) | (1.130, -1.939, -26.543) |
| | UL | (0.0, 24.58, 0.0) | (-0.100, -2.001, -1.997) |
| I3 | LL | (0.0, 0.0, 0.0) | (2.361, 23.024, -26.543) |
| | LR | (24.58, 0.0, 0.0) | (1.131, 23.086, -1.997) |
| | UR | (24.58, 24.58, 0.0) | (-0.100, -1.459, -1.997) |
| | UL | (0.0, 24.58, 0.0) | (1.130, -1.521, -26.543) |
| S0 | LL | (0.0, 0.0, 0.0) | (0.744, -81.170, -59.170) |
| | LR | (24.58, 0.0, 0.0) | (0.353, -56.597, -59.170) |
| | UR | (24.58, 24.58, 0.0) | (0.353, -56.597, -34.594) |
| | UL | (0.0, 24.58, 0.0) | (0.744, -81.170, -34.594) |
| S1 | LL | (0.0, 0.0, 0.0) | (0.348, -56.133, -59.170) |
| | LR | (24.58, 0.0, 0.0) | (0.099, -31.559, -59.170) |
| | UR | (24.58, 24.58, 0.0) | (0.099, -31.559, -34.594) |
| | UL | (0.0, 24.58, 0.0) | (0.348, -56.133, -34.594) |
| S2 | LL | (0.0, 0.0, 0.0) | (0.096, -31.100, -59.170) |
| | LR | (24.58, 0.0, 0.0) | (-0.011, -6.524, -59.170) |
| | UR | (24.58, 24.58, 0.0) | (-0.011, -6.524, -34.594) |
| | UL | (0.0, 24.58, 0.0) | (0.096, -31.100, -34.594) |
| S3 | LL | (0.0, 0.0, 0.0) | (-0.011, -6.035, -59.170) |
| | LR | (24.58, 0.0, 0.0) | (0.024, 18.541, -59.170) |
| | UR | (24.58, 24.58, 0.0) | (0.024, 18.541, -34.594) |
| | UL | (0.0, 24.58, 0.0) | (-0.011, -6.035, -34.594) |
| S4 | LL | (0.0, 0.0, 0.0) | (0.026, 18.970, -59.170) |
| | LR | (24.58, 0.0, 0.0) | (0.208, 43.545, -59.170) |
| | UR | (24.58, 24.58, 0.0) | (0.208, 43.545, -34.594) |
| | UL | (0.0, 24.58, 0.0) | (0.026, 18.970, -34.594) |
| S5 | LL | (0.0, 0.0, 0.0) | (0.208, 43.986, -59.170) |
| | LR | (24.58, 0.0, 0.0) | (0.528, 68.560, -59.170) |
| | UR | (24.58, 24.58, 0.0) | (0.528, 68.560, -34.594) |
| | UL | (0.0, 24.58, 0.0) | (0.208, 43.986, -34.594) |

The HRC instrument has two detectors, the HRC-S and the HRC-I. The HRC-I has a single ‘chip’ or segment/microchannel plate pair (CHIP ID = 0, name HRC-I) while the HRC-S has three (CHIP ID = 1,2,3; name HRC-S1,S2,S3; HRC team segment designation +1, 0, -1). We define an HRC-I chip plane which is 16384 pixels square; (not all of these pixels correspond to actual readable values); the HRC-S chips are 4096 x 16456 pixels. The pixel size is 0.0064294 mm.

| Name | ID | CHIP size (pix) | Pixel size (μ) | CHIP size (mm) |
|--------|----|-----------------|----------------------|-------------------|
| HRC-I | 0 | 16384 x 16384 | 6.429 x 6.429 | 105.333 x 105.333 |
| HRC-S1 | 1 | 4096 x 16456 | 6.250 x 6.429 | 25.600 x 105.802 |
| HRC-S2 | 2 | 4096 x 16456 | 6.250 x 6.429 | 25.600 x 105.802 |
| HRC-S3 | 3 | 4096 x 16456 | 6.250 x 6.429 | 25.600 x 105.802 |

The corners of these logical chip planes are located in the LSI coordinate system as follows; these are calculated by placing the HRC-S origin (default aimpoint) at 4.0mm to +LSI Y of the overall detector center and using the chip sizes calculated above together with the designed S1 and S3 chip tilts in the X,Y plane. Note that S2 is no longer centered around the detector center, since its edges are determined by the measured gap locations.

Table 4: HRC chip (i.e. grid) corner locations in LSI coordinates

| Chip | Corner | CPC coords | HRC-I,S LSI coords |
|--------|--------|-------------------------------|--------------------------------|
| HRC-I | LL | (0.000 , 0.000 , 0.000) | (0.000 , 0.000 , 74.482) |
| HRC-I | LR | (105.339 , 0.000 , 0.000) | (0.000 , 74.482 , 0.000) |
| HRC-I | UR | (105.339 , 105.339 , 0.000) | (0.000 , 0.000 , -74.482) |
| HRC-I | UL | (0.000 , 105.339 , 0.000) | (0.000 , -74.482 , 0.000) |
| HRC-S1 | LL | (0.000 , 0.000 , 0.000) | (2.644 , 161.949 , -13.167) |
| HRC-S1 | LR | (26.334 , 0.000 , 0.000) | (2.644 , 161.949 , 13.167) |
| HRC-S1 | UR | (26.334 , 105.802 , 0.000) | (0.000 , 56.180 , 13.167) |
| HRC-S1 | UL | (0.000 , 105.802 , 0.000) | (0.000 , 56.180 , -13.167) |
| HRC-S2 | LL | (0.000 , 0.000 , 0.000) | (0.000 , 56.180 , -13.167) |
| HRC-S2 | LR | (26.334 , 0.000 , 0.000) | (0.000 , 56.180 , 13.167) |
| HRC-S2 | UR | (26.334 , 105.802 , 0.000) | (0.000 , -49.622 , 13.167) |
| HRC-S2 | UL | (0.000 , 105.802 , 0.000) | (0.000 , -49.622 , -13.167) |
| HRC-S3 | LL | (0.000 , 0.000 , 0.000) | (0.000 , -49.622 , -13.167) |
| HRC-S3 | LR | (26.334 , 0.000 , 0.000) | (0.000 , -49.622 , 13.167) |
| HRC-S3 | UR | (26.334 , 105.802 , 0.000) | (2.253 , -155.400 , 13.167) |
| HRC-S3 | UL | (0.000 , 105.802 , 0.000) | (2.253 , -155.400 , -13.167) |

3.2 Tiled detector (TDET) coordinates)

The unphysical tiled coordinate system is defined here. Each system has a label used to distinguish it from previous choices of definition.

$$\begin{pmatrix} TDETX \\ TDETY \end{pmatrix} = \Delta_i \begin{pmatrix} 1 & 0 \\ 0 & H_i \end{pmatrix} \begin{pmatrix} \cos \theta_i & \sin \theta_i \\ -\sin \theta_i & \cos \theta_i \end{pmatrix} \begin{pmatrix} CHIPX - 0.5 \\ CHIPY - 0.5 \end{pmatrix} + \begin{pmatrix} X0_i + 0.5 \\ Y0_i + 0.5 \end{pmatrix} \quad (5)$$

where the values of H_i , Δ_i and θ_i are different for each chip. H_i gives the handedness of the planar rotation and has values +1 or -1, Δ_i gives the sub-pixel resolution factor which is always 1 in the current implementation, and θ_i gives the rotation angle of the chip axes with respect to the detector coordinate axes.

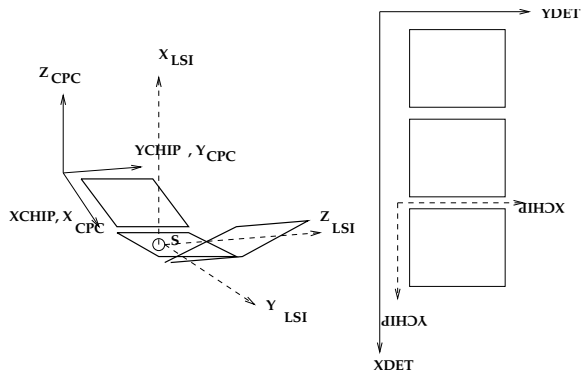


Figure 11: The relationship between CHIP and Tiled Detector coordinates.

For HRC-S, the tiled system coincides with the continuous (degapped, discontinuity-corrected) U,V system used by the instrument team. There are electronic discontinuities in V between the HRC segments, so that the degapped instrument coordinates $vpos_d$ are corrected to continuous instrument coordinates $vpos$ and then to CHIPY and TDETY. The relationship for HRC-I is $CHIPX = vpos_d + 1$, $CHIPY = vpos_d + 1$ while for HRC-S, $CHIPX = vpos_d + 1$, and $CHIPY$ as tabulated below. Users who are not members of the HRC instrument team probably don't need to worry about the $vpos$, $vpos$ coordinates.

Table 5: HRC-S discontinuities

| $vpos_d$ | $vpos$ | CHIPY | TDETY |
|-----------------|---------------|--------------------|-----------------|
| 0-16444.5 | $vpos_d$ | $vpos_d + 12.5$ | CHIPY - 12.0 |
| 16444.5-16459.9 | $vpos_d$ | 16456.4 | |
| 16459.9-32916.4 | $vpos_d - 16$ | $vpos_d - 16459.5$ | CHIPY + 16444.0 |
| 32916.4-32930.0 | $vpos_d - 16$ | 0.5 | |
| 32930.0+ | $vpos_d - 29$ | $vpos_d - 32929.5$ | CHIPY + 32900.0 |

Table 6: Tiled Detector Plane systems

| System | Size | X Center, Y Center | Use |
|---------------|---------------|--------------------|----------|
| AXAF-ACIS-2.2 | 8192 x 8192 | (4096.5, 4096.5) | Standard |
| AXAF-HRC-2.3I | 16384 x 16384 | (8192.5, 8192.5) | HRC-I |
| AXAF-HRC-2.6S | 49368 x 4096 | (24684.5, 2048.5) | HRC-S |

Table 7: Parameters of Tiled Detector Coordinate definitions

| Tiled System | Chip | θ_i | Δ_i | $X0_i$ | $Y0_i$ | H_i |
|---------------------|---------|------------|------------|---------|---------|-------|
| AXAF-ACIS-2.2 | ACIS-I0 | 90 | 1 | 3061.0 | 5131.0 | 1 |
| AXAF-ACIS-2.2 | ACIS-I1 | 270 | 1 | 5131.0 | 4107.0 | 1 |
| AXAF-ACIS-2.2 | ACIS-I2 | 90 | 1 | 3061.0 | 4085.0 | 1 |
| AXAF-ACIS-2.2 | ACIS-I3 | 270 | 1 | 5131.0 | 3061.0 | 1 |
| AXAF-ACIS-2.2 | ACIS-S0 | 0 | 1 | 791.0 | 1702.0 | 1 |
| AXAF-ACIS-2.2 | ACIS-S1 | 0 | 1 | 1833.0 | 1702.0 | 1 |
| AXAF-ACIS-2.2 | ACIS-S2 | 0 | 1 | 2875.0 | 1702.0 | 1 |
| AXAF-ACIS-2.2 | ACIS-S3 | 0 | 1 | 3917.0 | 1702.0 | 1 |
| AXAF-ACIS-2.2 | ACIS-S4 | 0 | 1 | 4959.0 | 1702.0 | 1 |
| AXAF-ACIS-2.2 | ACIS-S5 | 0 | 1 | 6001.0 | 1702.0 | 1 |
| HRC: old convention | | | | | | |
| AXAF-HRC-2.3I | HRC-I | 90 | 1 | 0.0 | 0.0 | -1 |
| AXAF-HRC-2.6S | HRC-S1 | 270 | 1 | 49368.0 | 0.0 | 1 |
| AXAF-HRC-2.6S | HRC-S2 | 270 | 1 | 32912.0 | 0.0 | 1 |
| AXAF-HRC-2.6S | HRC-S3 | 270 | 1 | 16456.0 | 0.0 | 1 |
| HRC: new convention | | | | | | |
| AXAF-HRC-2.4I | HRC-I | 0 | 1 | -1.0 | 0.0 | 1 |
| AXAF-HRC-2.7S | HRC-S1 | 0 | 1 | 0.0 | -12.0 | 1 |
| AXAF-HRC-2.7S | HRC-S2 | 0 | 1 | 0.0 | 16444.0 | 1 |
| AXAF-HRC-2.7S | HRC-S3 | 0 | 1 | 0.0 | 32900.0 | 1 |

3.3 Relative positions of instruments

The location of the origins of the LSI system for each instrument are given in STT coordinates in the table below. The in-flight calibration will be refined when angular misalignments in the system are measured.

Table 8: Location of instrument origin on Translation Table

| Values of LSI origins OLSI in STT system, prelaunch | | |
|---|---------------------|--------------------------|
| Instrument | Prelaunch estimate | Dec 1999 calibration |
| ACIS origin | (0.0, 0.0, 237.4) | (0.684, 0.750, 236.552) |
| HRC-I origin | (0.15, 0.0, -126.6) | (1.040, 0.978, -132.028) |
| HRC-S origin | (0.10, 0.0, -250.1) | (1.533, 1.530, -251.437) |

3.4 Aimpoints

Unless the observer specifies an offset, the SIM will be placed at one of four default locations. The table below gives the SIM values (STF coordinates of the instrument table origin) for each of these aimpoints. Recall that in general the SIM can also be moved in X and Z to other aimpoints.

The SIM Z motion is commanded in ‘TSC motor steps’ which are 2.5143153 microns per Z step. The focus stage, FA, mapping from motor step to SIM X is a degree 6 polynomial.

$$SIM Z(mm) = -0.00251431530156TSC$$

and

$$SIM X(mm) = \sum_{n=0}^6 c_n \left(\frac{FA}{10^4} \right)^n$$

where

Table 9: Coefficients of FA stage motor step to SIM X position

| n | c_n |
|---|-------------|
| 0 | 0.0 |
| 1 | 14.7906994 |
| 2 | 3.5723322 |
| 3 | -1.08492544 |
| 4 | 0.39803832 |
| 5 | 0.529336 |
| 6 | 0.1020064 |

Table 10: SIM hard limits

| | Min | Max |
|-------|----------|----------|
| SIM X | -28.965 | +16.783 |
| SIM Z | -262.200 | +263.359 |

The X coordinates of the offsets may be regarded as estimates of the instrument origin X positions, and may be added to the instrument origin values in later revisions of the processing system. For the ACIS origin, we note that a SIM X position of -0.684mm is used for the ACIS-S3 chip aimpoint which is within 0.002 mm of the ACIS LSI (PSU) X origin, and we therefore adopt this as the origin of the ACIS system. The fact that the ACIS-I aimpoint is 0.1mm different in X is taken into account by the different X values of the corners of the ACIS-I chips relative to ACIS-S.

Table 11: SIM position offsets for nominal focus positions

| Values of $P_{STF}(\Sigma)$ | | | | |
|-----------------------------|--------------|-------------------------|-------------------------|-----------------|
| | ODB offset | | CHIP | TDET |
| | Motor steps | mm | pixel | |
| AI2 ACIS-I offset | -536, 92905 | (-0.782, 0.0, -233.592) | ACIS-I3 (984.4, 994.8) | 4137.2, 4045.4 |
| AS1 ACIS-S offset | -468, 75620 | (-0.684, 0.0, -190.133) | ACIS-S3 (220.7, 531.8) | 4137.7, 2233.8 |
| HI1 HRC-I offset | -716, -50505 | (-1.040, 0.0, 126.985) | HRC-I (7529.9, 7745.0) | 7528.9, 7744.0 |
| LETG HRC-S offset | -991, -99612 | (-1.430, 0.0, 250.456) | HRC-S2 (2201.0, 8976.5) | 2200.0, 25420.5 |

3.5 Detector and sky pixel plane systems

In this section we specify the pixel systems used to report detector and sky coordinates. We decided to use the mean actual instrument pixel sizes for these systems. Thus, the size of a physical HRC-I pixel at the nominal focal distance of 10061.0 mm is 0.132 arcseconds, so 0.132 arcseconds is defined as the FP-2.1 pixel size (even if the detector is moved well off focus). The HRC-S detector has a maximum linear extent of over 48500 pixels. When making sky coordinates for such a detector, we must define a square pixel plane (to allow for the roll angle). We choose a 65536 pixel sided plane, defined as FP-2.3. This plane has a total of 4.3 gigapixels, slightly more than can fit in a 4-byte signed integer. A 2-byte integer counts image would then have a file size of 8.0 gigabytes. We therefore recommend not making full resolution full frame image files in this coordinate system; the CXC data analysis system may be used to make full resolution images of small areas and low resolution images of the full field.

The adopted focal length on orbit, based on ray trace simulations optimized to fit ground calibration data (P. Zhao, private communication) was reported to be

10061.65mm

This value is currently under review. The measured plate scale gives a provisional effective focal length of around 10070 mm.

Here are the current flight pixel systems:

| System | Pixel size (mm) | Pixel size (arcsec) | X0, Y0 | Full size | Purpose |
|-------------|--------------------|------------------------|---------|---------------|--------------|
| AXAF-FP-1.1 | 0.0240 | 0.49200 | 4096.5 | 8192 x 8192 | Flight ACIS |
| AXAF-FP-2.1 | 0.006427 | 0.13175 | 16384.5 | 32768 x 32768 | Flight HRC-I |
| AXAF-FP-2.3 | 0.006427 | 0.13175 | 32768.5 | 65536 x 65536 | Flight HRC-S |
| AXAF-FP-2.1 | 0.006429 | 0.13180 | 16384.5 | 32768 x 32768 | Flight HRC-I |
| AXAF-FP-2.3 | 0.006429 | 0.13180 | 32768.5 | 65536 x 65536 | Flight HRC-S |

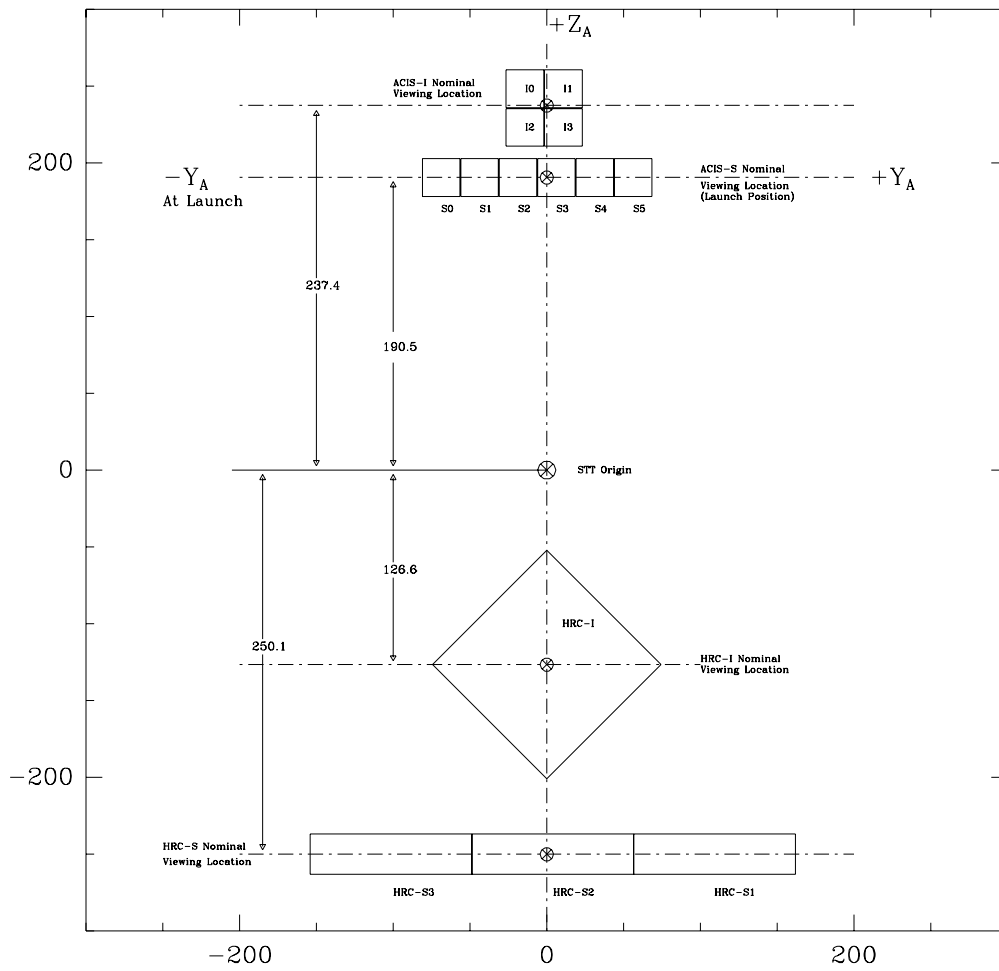


Figure 12: The AXAF SIM Translation Table, showing the flight focal plane instruments to scale. Distances are in mm. Coordinate system is AXAF-STT-1.0.

3.6 Remaining issues

There is a remaining uncalibrated rotation of the HRC-I of order 0.3 degree; and an uncertainty in the plate scale and effective focal length of order 0.2 percent.

4 Summary

We have discussed the derivation of celestial coordinates for Chandra data and presented coordinate systems suitable for description of instrumental, telescope-related and celestial effects. The formalism is sufficiently general that it should be applicable to other missions by appropriately changing the numerical values in section 3. In Paper 2, we discuss derivation of the alignments and the aspect solution. In Paper 3, coordinate systems useful for analysing dispersed grating data are presented.

We thank Ian Evans, Tom Aldcroft, Maxim Markevitch, Kenny Glotfelty, Janet DePonte, Steve Murray, Brian McNamara and Martin Elvis for useful discussions, and Helen He for implementing the software routines used to apply the coordinate transforms in the Chandra data processing system.

Contents

| | | |
|----------|---|-----------|
| 1 | Introduction | 1 |
| 1.1 | Fundamentals | 1 |
| 1.2 | The chip, detector and sky coordinate systems | 2 |
| 1.3 | Pixel convention | 7 |
| 2 | Transformation equations and intermediate coordinate systems | 7 |
| 2.1 | Sky coordinates to celestial coordinates | 7 |
| 2.2 | Detector coordinates to celestial coordinates | 8 |
| 2.3 | Chip coordinates to detector coordinates | 9 |
| 2.4 | Detector coordinates and off-axis angles | 12 |
| 2.5 | Dithered-corrected chip (DC) and chip-aligned source-centered sky (CSC) coordinates | 12 |
| 2.6 | Source-centered coordinates | 14 |
| 3 | In-flight numerical values for Chandra | 15 |
| 3.1 | ACIS and HRC chip locations | 15 |
| 3.2 | Tiled detector (TDET) coordinates) | 17 |
| 3.3 | Relative positions of instruments | 19 |
| 3.4 | Aimpoints | 20 |
| 3.5 | Detector and sky pixel plane systems | 21 |
| 3.6 | Remaining issues | 23 |
| 4 | Summary | 23 |

List of Tables

| | | |
|----|--|----|
| 2 | ACIS Chip corner locations in ACIS-I LSI coordinates | 16 |
| 4 | HRC chip (i.e. grid) corner locations in LSI coordinates | 17 |
| 5 | HRC-S discontinuities | 18 |
| 6 | Tiled Detector Plane systems | 18 |
| 7 | Parameters of Tiled Detector Coordinate definitions | 18 |
| 8 | Location of instrument origin on Translation Table | 19 |
| 9 | Coefficients of FA stage motor step to SIM X position | 20 |
| 10 | SIM hard limits | 20 |
| 11 | SIM position offsets for nominal focus positions | 20 |

List of Figures

| | | |
|---|---|---|
| 1 | An image in detector coordinates, showing a dithered source. | 3 |
| 2 | The same image in sky coordinates, with aspect applied. The source is PKS 0637-752, a quasar with a newly discovered X-ray jet. | 4 |
| 3 | The same image showing DETX versus time along the x axis | 4 |
| 4 | The same image showing the X coordinate on the y axis versus time along the x axis. The jet is visible at larger X values. | 5 |
| 5 | The different pixel plane coordinate systems. Distorting effects are highly exaggerated. | 6 |
| 6 | Imaging the sky in LSI coordinates | 7 |

| | | |
|----|---|----|
| 7 | Pixel convention. | 7 |
| 8 | The relationship between CHIP, LSI and STT coordinates. | 9 |
| 9 | The instrument compartment (dashed line) may be misaligned with the telescope mirrors. At calibration, this misalignment (highly exaggerated here) may be significant and variable as the mirror is tilted with respect to the instruments. The instrument bench moves with respect to the instrument compartment, as indicated by the arrow. | 10 |
| 10 | The relationship between STT and STF coordinates. | 11 |
| 11 | The relationship between CHIP and Tiled Detector coordinates. | 18 |
| 12 | The AXAF SIM Translation Table, showing the flight focal plane instruments to scale. Distances are in mm. Coordinate system is AXAF-STT-1.0. | 22 |